Zinc Chloride as a Catalyst in Hydrothermal Carbonization of Cocoa Pods Husk

Understanding the Effect of Different Carbonization Temperature and ZnCl$_2$ Concentration

Ratna Frida Susanti[1]*, Raden Gamelli Rachma Dewi Wiratmadja[1], Kevin Cleary Wanta[1], Arenst Andreas Arie[1], Hans Kristianto[1]**

[1] Department of Chemical Engineering, Faculty of Industrial Technology, Parahyangan Catholic University, Ciumbuleuit 94, Bandung 40141, Indonesia
* First corresponding author, e-mail: santi@unpar.ac.id
**Second corresponding author, e-mail: hans.kristianto@unpar.ac.id

Abstract

In this study, we have successfully synthesized a high surface area of activated carbons (ACs) from cocoa pod husk (CPH) by using a combination of hydrothermal carbonization (HTC) and chemical activation in the presence of ZnCl$_2$ as both of catalyst as well as activating agent. During HTC, the effect of HTC temperature (200 and 225 °C) and ZnCl$_2$ to biomass mass ratio (1:1, 2:1, 3:1) as a catalyst to the characteristics of the obtained hydrochar (HC) and ACs were investigated. The obtained hydrochar (HCs) was then processed by using ZnCl$_2$ chemical activation with a fixed HC to ZnCl$_2$ mass ratio of 1:4 and the mixture was pyrolyzed at 600 °C for 1 h under an inert atmosphere. The results showed that the addition of catalyst during HTC presented different AC morphology, where the carbon samples were decorated with carbon microspheres. An increase of surface area was observed, where the ACs synthesized from catalyzed HC at biomass to ZnCl$_2$ ratio of 1:3 at temperature 200 °C gave a higher surface area of 1954 m^2/g compared to that of without catalyst (1165 m^2/g). The catalysis effect was more profound at the HTC temperature of 200 °C compared to 225 °C, as reflected in the significant increase of AC surface area. The addition of a catalyst creates ACs with narrow pore distribution compared to that of synthesized in the absence of a catalyst. It was also observed that the ACs from catalyzed hydrochar possessed higher oxygenated functional groups (OFG) than those without catalysts.

Keywords

activated carbon, chemical activation, cocoa pod husk, hydrothermal carbonization, ZnCl$_2$

1 Introduction

Cocoa (*Theobroma cacao* L.) is a tropical commodity crop from which cocoa beans are obtained. The top 5 cocoa-producing countries include Ivory Coast, Ghana, Indonesia, Nigeria, and Cameroon. In 2020, around 4.7 million tons of cocoa beans were produced globally [1]. From cocoa beans, various derivative products can be obtained, including cocoa nibs, cocoa mass, cocoa butter, and cocoa powder [2]. The cocoa bean makes up 33% weight of cocoa fruit, leaving 67% of the unused pods, known as cocoa pod husk (CPH) [3]. Furthermore, according to Vriesmann et al. [4], ten tons of CPH are generated per ton of dry cocoa beans, resulting in a huge amount of agricultural waste that needs to be managed. On the other hand, CPH contains relatively high cellulose (23.8%), hemicelluloses (8.2%), and lignin (33.4%) [5] which makes it a suitable source for the synthesis of activated carbon (AC) [6].

Conversion of CPH into carbon materials such as hard carbon as well as activated carbon has been attempted by our groups [5, 7] as well as several other reports. Our group is the first who investigate the ACs synthesis from CPH by hydrothermal carbonization (HTC) and chemical activation [7]. We obtained a surface area of 1694.91 m^2/g which is larger than the one produced via pyrolysis or other methods. In those works, we investigated the effect of different HTC temperatures on the characteristics of activated carbon produced. Several advantages of HTC are its suitability to treat biomass with high water content, lower operation

temperature, and unique properties, such as high oxygenated functional groups of the resulting product [8]. At HTC condition (180–250 °C), the water is at the subcritical phase, in which the ion product constant is higher compared to that at room temperature, making an acidic environment that is suitable for a hydrolysis reaction. It is generally accepted that the hydrolysis reaction is the initial step in HTC lignocellulose conversion, followed by dehydration, decarboxylation, polymerization, and aromatization [9]. During HTC, several organic acids are also produced as the by-product that can also act as hydrolysis catalysts, making the HTC process usually done without a catalyst addition.

Even so, the introduction of additives in the HTC process is known to be able to influence the properties of hydrochar (HC) such as enhanced degree of carbonization, surface modification, and inclusion of heteroatoms that could be beneficial in the AC synthesis [10]. The addition of acids such as citric acid [11], ascorbic acid [12], HCl, and HNO_3 [13] have been reported in the synthesis of hydrochar from various biomass. Furthermore, several metal salts such as $CeCl_3$ [14–16], $FeCl_3$ [17], CsCl, $SnCl_2$ [18] have been utilized as HTC catalysts. The utilization of Zinc Chloride ($ZnCl_2$) as an HTC catalyst has also been reported by several researchers [18–22]. However, to the best of the authors' knowledge, the combined effect of temperature and $ZnCl_2$ (as a catalyst) to biomass mass ratio in the HTC process to the ACs characteristics have never been reported before in CPH conversion.

In this study, we investigated the effect of $ZnCl_2$ as a catalyst in the HTC process of CPH. The HTC was done at various CPH to $ZnCl_2$ mass ratios and HTC temperatures. The obtained HCs were subsequently activated by using a chemical activation process with $ZnCl_2$ as an activating agent. The physicochemical characteristics of the HCs and ACs carbon products were analyzed and compared with the ones without HTC catalysts. We proved that the addition of catalyst and carbonization temperature were closely related.

2 Experimental
2.1 Preparation of CPH
CPH was obtained from a cocoa plantation in Indonesia and was used as a biomass precursor in this study. CPH was repeatedly washed using distilled water to remove impurities, followed by oven-drying at 105 °C for 24 h. The dried CPH was then crushed, ground, and sieved to obtain CPH powder with a size of −30 + 50 mesh (±0.446 mm). The obtained CPH powder was kept dry until used.

2.2 Synthesis of hydrochar
Hydrochar was synthesized through high-temperature carbonization (HTC) by adding $ZnCl_2$ as a catalyst for carbonization. In each experiment, a 4 g of CPH powder was mixed with 80 mL of $ZnCl_2$ (p.a., Merck, Germany) solution with various $ZnCl_2$ to CPH mass ratios (1:1, 2:1, 3:1). The mixture was mixed by using a magnetic stirrer for 15 min followed by ultrasonic treatment for another 30 min. The mixture was then hydrothermally carbonized by using a 100 mL of an autoclave with a Teflon liner in an oven at temperatures of (200 and 225 °C) for 24 h. After HTC, the obtained HC was then separated from the liquid product and washed using ethanol (96%, Bratachem, Indonesia) and distilled water repeatedly. The HC was then oven dried at 105 °C for 24 h. As a comparison, a similar experiment was also done by using only distilled water as the HTC medium. The HC sample was coded as HC-x-y, where x is the HTC temperature, and y is the ratio of $ZnCl_2$.

2.3 Synthesis of activated carbon
Hydrochar obtained from HTC was activated by chemical activation, using the same chemical ($ZnCl_2$) as activating agent. Synthesis of ACs was done by impregnating HC/$ZnCl_2$ with a mass ratio of 1:4. The mixture was mixed using a magnetic stirrer for 15 min and left to impregnate for 24 h. The mixture was then oven-dried at 80 °C for 24 h. The pyrolysis process was done by using a tubular furnace at 600 °C for 1 h under an inert N_2 atmosphere. The obtained ACs were washed using 0.1 M HCl solution followed by distilled water until neutral pH. The washed ACs were then dried at 105 °C for 24 h. The dried ACs were then stored and kept dry in a sealed container. The ACs sample are denoted as AC-x-y where x is the carbonization temperature and y is the catalyst ratio during HTC. The commercial AC (Merck, pa, CAS#7440-44-0) was used as a comparison.

2.4 Characterization
The obtained HCs and ACs were characterized by several methods. The yield of HCs and ACs was obtained by gravimetric. The scanning electron microscope (SEM, Hitachi SU3500, Japan, and JEOL JSM 6510-A, Japan) was used to observe the morphology of the samples. The functional groups of HCs and ACs were characterized using Fourier Transform Infra-Red Spectroscopy (FTIR, Prestige 21 Shimadzu Instruments) with KBr pellet method (carbon/KBR ratio is 15/175 mg). The pore characteristics were characterized using an N_2 adsorption-desorption study at

77K (Micromeritics TriStar II). The crystallinity of ACs was characterized using X-ray diffraction (XRD, Bruker D8 Advance, USA).

3 Results and discussion
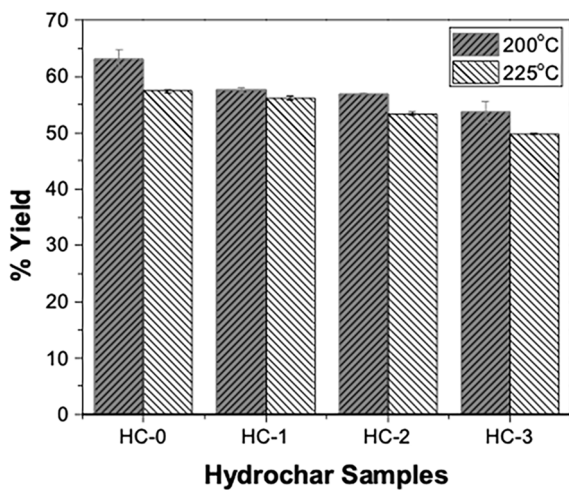
3.1 Yield of HCs and ACs

The effect of the $ZnCl_2$ catalyst on the HCs yield is presented in Fig. 1 (a). An increase of catalyst to CPH ratio from HC-0 to HC-3 lowered the HC yield from 63.16 to 53.6% and 57.4% to 49.8% for HTC temperature from 200 to 225 °C respectively. The $ZnCl_2$ is known as a Lewis acid that could act as a catalyst during the HTC process. The catalyst would accelerate the reaction of cellulose, hemicelluloses, and lignin decomposition into gaseous products such as CO and CO_2, thus decreasing the yield of solid products. Furthermore, the HTC-225 also showed a lower yield compared to HTC-200 due to a higher devolatilization rate that resulted in more gaseous products at a higher HTC temperature [23]. Similar trends have been previously reported [6, 24, 25].
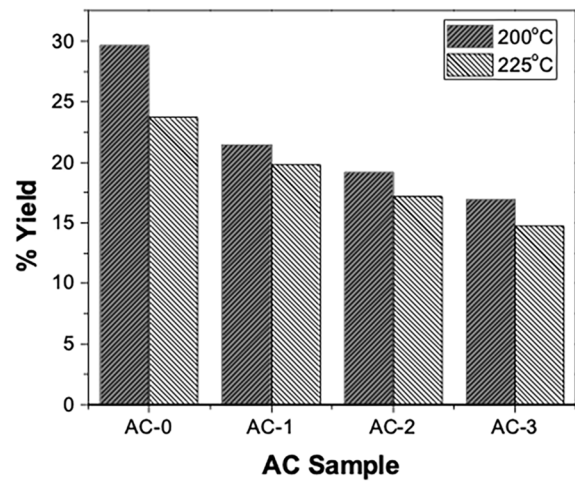
The effect of the HTC catalyst on the yield of ACs is presented in Fig. 1 (b). An increase in the HTC catalyst ratio also shows decreasing the ACs yield. It is known that during chemical activation, $ZnCl_2$ would inhibit tar formation and promote the decomposition of precursor to volatile gases that result in a pores formation [26]. An increase in $ZnCl_2$ ratio during the HTC process facilitated more lignocellulose decomposition [27], and facilitated the chemical activation, producing more pores which contributed to the lower yield.
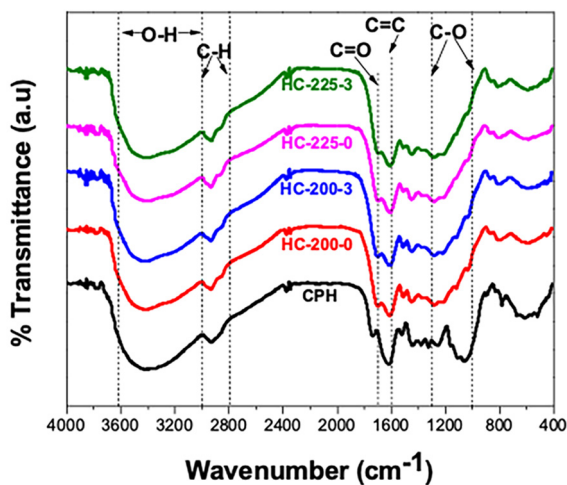
3.2 Functional groups of HC and AC

Observation of functional groups in the CPH, HC, and AC are presented in Fig. 1 (c), (d). Several notable peaks from the CPH spectrum are the O–H stretching around
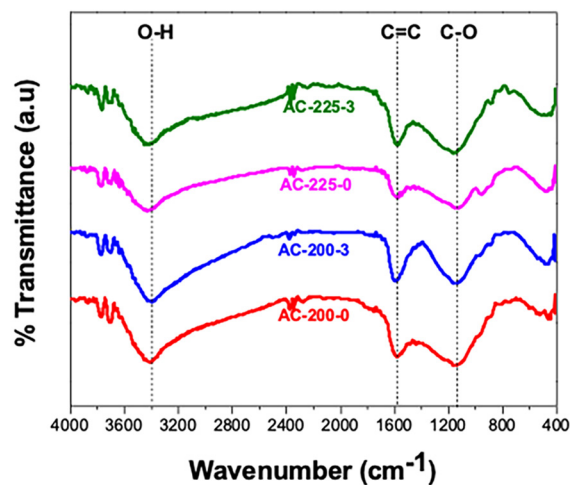

(a)

(b)

(c)

(d)

Fig. 1 Percentage of (a) HCs yield, (b) ACs samples and FTIR spectra of (c) CPH and HCs, (d) ACs samples at various catalyst ratios and HTC temperature

3000–3600 cm^{-1} due to absorbed moisture in CPH, C–H vibrational stretching around 2800–3100 cm^{-1}, the C=O stretching at 1760 cm^{-1} and C=C stretching at ~1600 cm^{-1} of hemicelluloses structure, and C–O stretching at ~1100 cm^{-1} from the glycosidic bond of cellulose structure, and peaks around 700–900 cm^{-1} that indicates lignin's C–H vibration [28, 29]. Upon carbonization, the chemical transformation of CPH to hydrochar could be observed clearly with changes of several notable peaks as shown in Fig. 1 (c). The C=O stretching was dominant in hydrochar than that of CPH showing the presence of aromatization and decomposition of dehydration product. Lower C–O stretching was due to the decomposition of lignocellulosic biomass resulting in lower C–O intensity in hydrochar. Spectra of C–H and O–H were similar however with lower intensity in hydrochar than CPH [7]. In the presence of $ZnCl_2$, the peaks of C=O and C=C were strengthened, indicating the stronger aromatization and decomposition of dehydration products in the presence of a catalyst, which agrees well with Li et al. [19]. Bands of O–H, C–H, and C–O were somewhat similar for all HCs.

The observation of functional groups of the AC samples is presented in Fig. 1 (d). It could be observed that the FTIR spectra of both samples are different from their respective HCs spectra. This indicates complete transformation of HC to AC after chemical activation. Several peaks are still present in the AC samples, namely the O–H stretching (300–3600 cm^{-1}) due to the presence absorbed water and phenolic functional groups, C=C stretching (~1570 cm^{-1}) of aromatic carbon ring structures, and C–O stretching (1150 cm^{-1}) that indicates carboxylic acid, lactone, and carbonyl functional groups [30, 31]. The C–H peak around 3000 cm^{-1} is no longer present in the AC samples due to removal of C–H structures during activation [32]. So do C=O stretching around 1760 cm^{-1} was disappear. Furthermore, it is notable that the AC-3 sample has higher oxygenated functional group content compared to AC-0, as reflected in the sharper peaks of O–H and C–O stretching. We hypothesize that this trend could happen due to the presence of $ZnCl_2$ during the HTC process has helped more complete conversion of CPH to carbon structures, with more volatiles already released during the HTC process, compared with one without catalyst. Thus, during chemical activation, the more functional groups could be preserved in the AC.

3.3 Morphology of HC and AC
Observation of the CPH and HC morphology is presented in Fig. 2 Fig. 2 (a) showed a well-defined cell wall structure of CPH that was decomposed after HTC. At HC-200-0,

a resemblance of CPH structure is still observable, but with more irregular morphology and destroyed cell walls. With the addition of $ZnCl_2$ catalyst (HC-200-3; Fig. 2 (c)) and an increase in HTC temperature (HC-225-0; Fig. 2 (d)), the cell wall structure could not be observed in the HC samples. Furthermore, on the HC-225-3 sample (Fig. 2 (e)) some cavities are observed on the surface, indicating initial pore formation after HTC.

Observation of AC samples' morphology using SEM is presented in Fig. 3. It shows that the AC-200-0 and AC-225-0 exhibited a similar morphology, in the form of a boulder shape with irregular cavities observed on the ACs surface. This morphology is commonly found on ACs from $ZnCl_2$ chemical activation due to $ZnCl_2$ evaporation during the activation process [33]. On the other hand, the AC-200-3 and AC-225-3 samples possessed different surface morphology, compared to the one without catalyst. It could be seen that agglomerates of carbon microspheres are decorating the ACs surface with random macro cavities. As previously explained, the presence of $ZnCl_2$ catalyst during the HTC process help the hydrolysis of the glycosidic bond of cellulose and hemicelluloses and resulted in abundant sugar monomers in the solution [6]. The monomers would further be transformed via dehydration, condensation, and polymerization into a spherical carbon structure [34]. Similar carbon microspheres structure due to catalyzed HTC has also been reported by previous researchers [6, 18].

3.4 Pore characteristics
The pore characteristics of HC samples are presented in Fig. 4 and Table 1. It shows that the HC isotherm curves exhibited a transient between type II and IV isotherm with H_3 type hysteresis loop that indicates the presence of macropores in the AC structure. Furthermore, from the BJH pore distribution curve (Fig. 4 (b)), it could be observed that the HC still possessed a wide mesopore distribution, with an average pore diameter of around 15 nm (Table 1). Furthermore, the effect of HTC temperature and catalyst concentration to the surface area and pore diameter of HCs were not significantly different, as seen in Table 1. This is also supported by relatively similar HC morphology in Fig. 2.

Observation of the nitrogen adsorption and desorption isotherm of ACs is presented in Fig. 5 (a), (b). It shows that all samples exhibited a type IV isotherm with H_2 type hysteresis loop, according to IUPAC classification that shows all ACs samples exhibited complex mesoporous structures [35], except for AC-200-3 and AC 225-0. The type IV isotherm typically shows a hysteresis loop
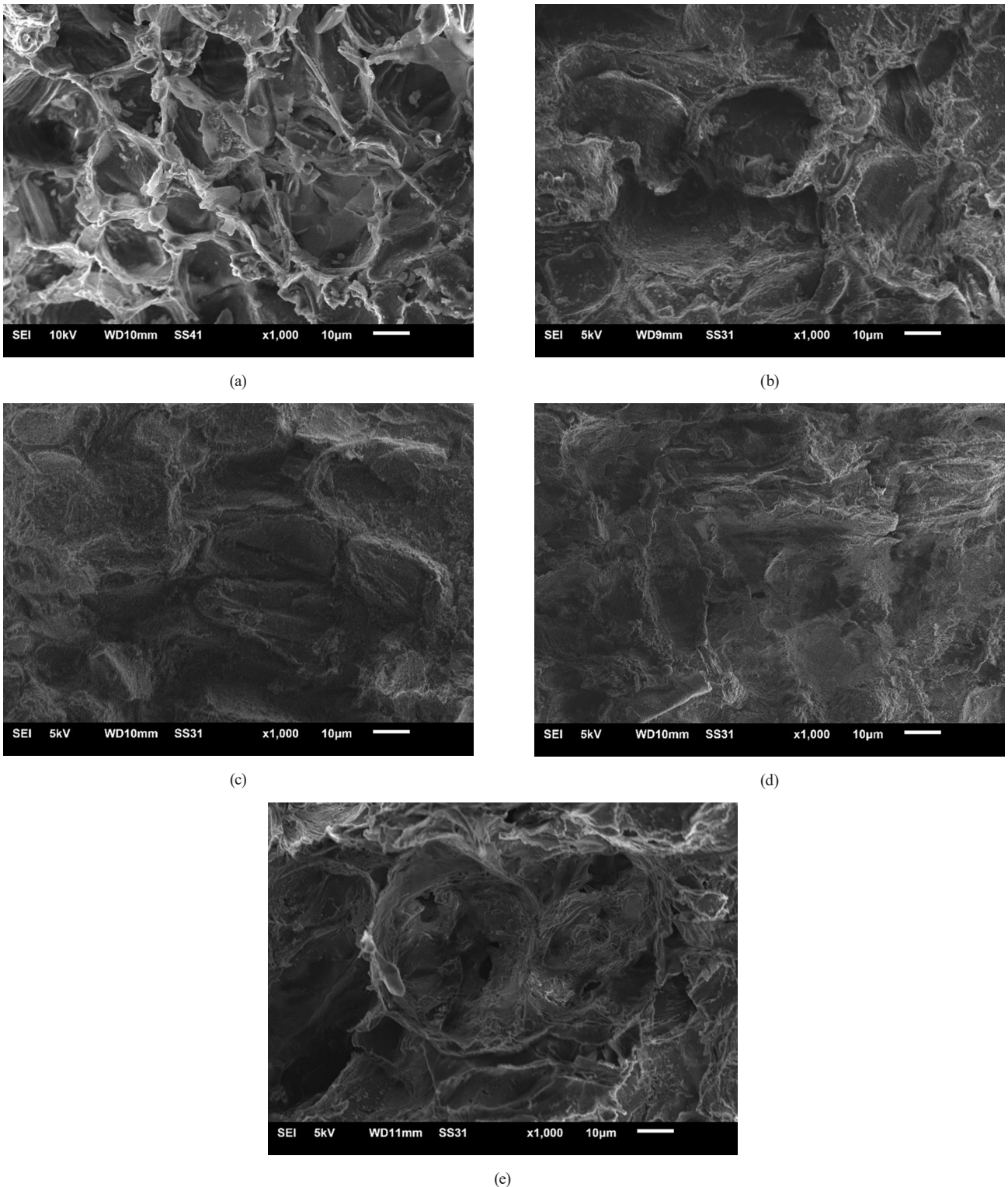
(a)

(b)

(c)

(d)

(e)

Fig. 2 Morphology of (a) CPH, (b) HC-200-0, (c) HC-200-3, (d) HC-225-0, and (e) HC-225-3

around relative pressure of 0.4 to 1.0 due to capillary condensation of nitrogen in the mesopores of AC structures during the desorption process. The step loops around 0.4–0.6 demonstrates these ACs samples possess uniform mesoporous structures [36]. This result is in accordance with the BJH pore distribution curve, presented

in Fig. 5 (e), (f), with more uniformly distributed pores around 2–5 nm. The AC-200-3 sample exhibited a typical type I isotherm that indicates a more dominant micropores structure of AC, as also reflected in the BJH distribution that is dominantly for pores <4 nm. A higher concentration of $ZnCl_2$ seems tends to increase the surface area by
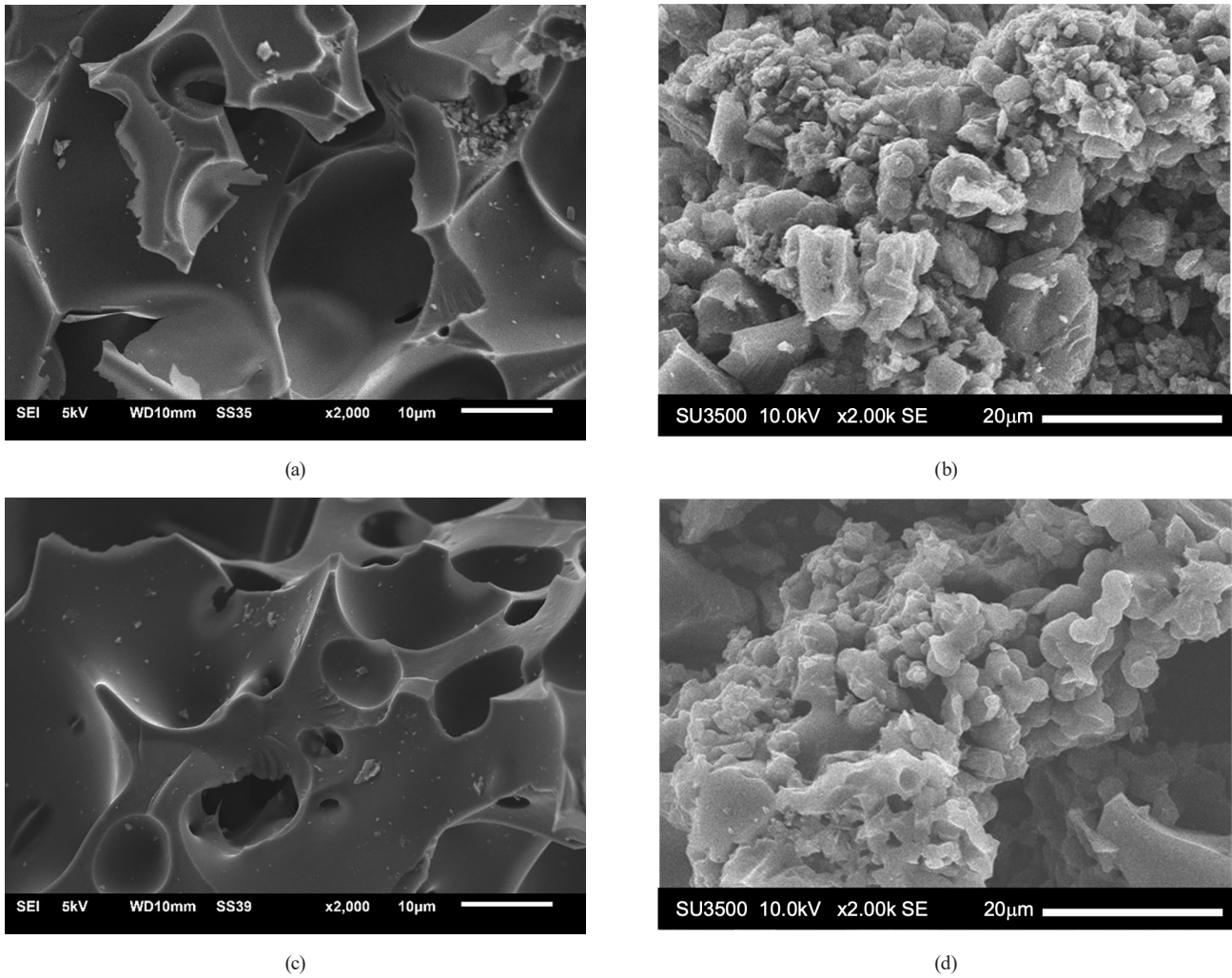
(a)

(b)

(c)

(d)

Fig. 3 Morphology of AC samples: (a) AC-200-0, (b) AC-200-3, (c) AC-225-0, and (d) AC-225-3
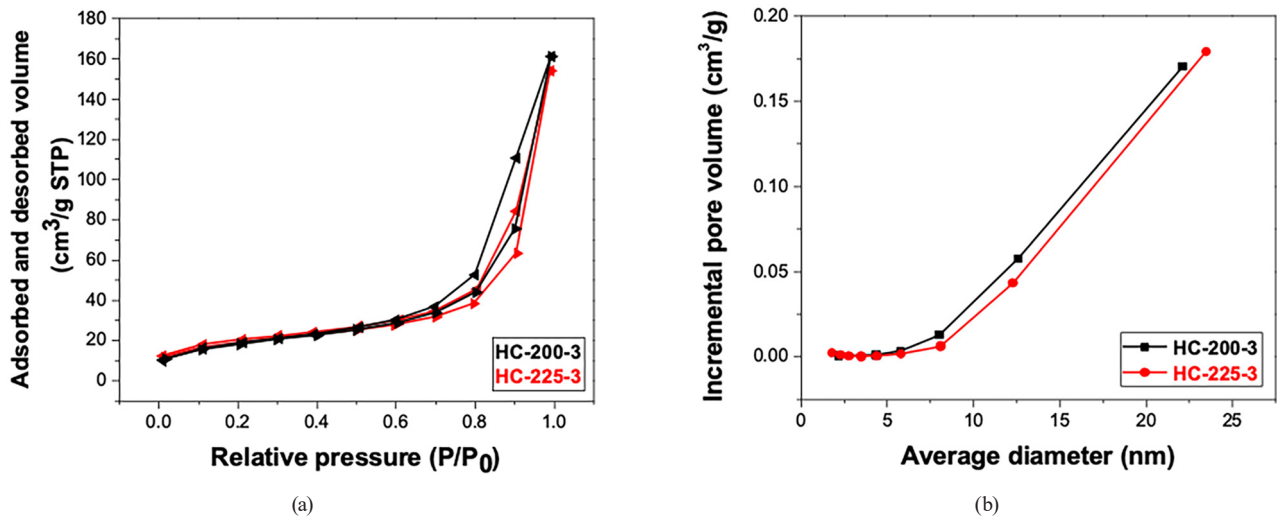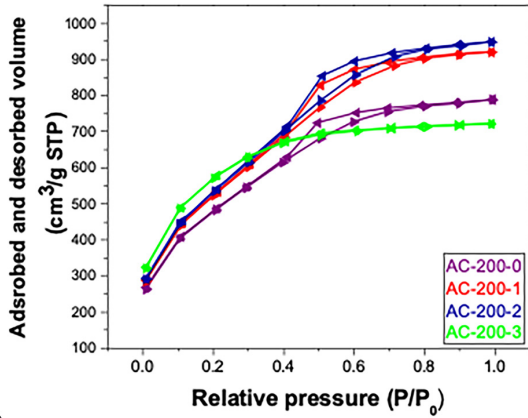

(a)

(b)

Fig. 4 (a) Isotherm adsorption-desorption plot and (b) BJH pore distribution for HCs samples

decreasing pore size. Furthermore, the AC-225-0 sample exhibited a transient between type II and IV isotherm with H_3 type hysteresis loop that indicates the presence of macropores in the AC structure which are not completely filled 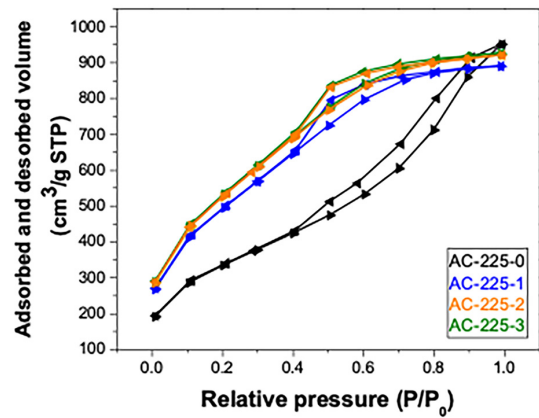with the pore condensate [37]. This statement is also in line with the wide pore distribution that is observed in the BJH analysis. The commercial AC as shown in Fig. 5 (c) exhibited a type IV isotherm with a type H_4 hysteresis loop. The more pronounced uptake at low P/P_0 was associated with the filling of the micropores [37].
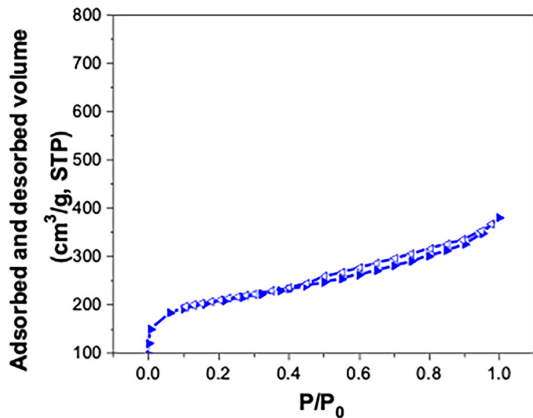
Table 1 Pore characteristics of HC samples

Sample	BET surface area (m²/g)	Average pore diameter (nm)
HC-200-3	63	15.8
HC-225-0	68	15.9
HC-225-1	63	17.5
HC-225-2	63	16.3
HC-225-3	65	14.7

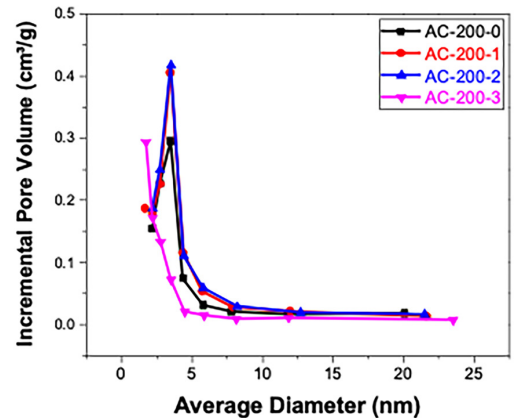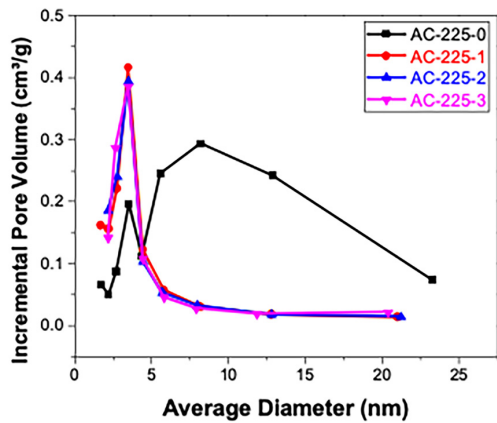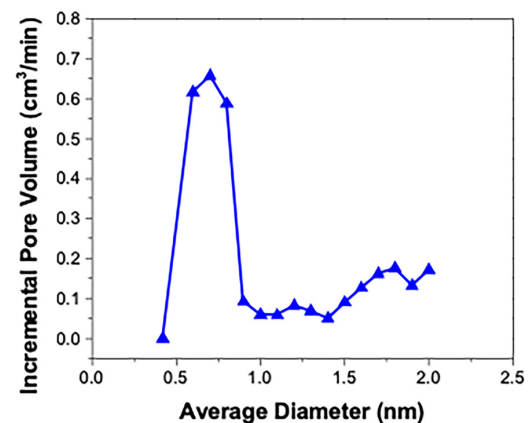**Fig. 5** Isotherm adsorption-desorption curve of (a) ACs synthesized at 200 °C, (b) ACs synthesized at 250 °C; (c) commercial AC and BJH pore distribution of (d) ACs synthesized at 200 °C, (e) ACs synthesized at 250 °C, (f) commercial AC

It is known that there are several roles of $ZnCl_2$ during the chemical activation process [38]. From room temperature to 160 °C the evaporation of water and dehydration of biomass by $ZnCl_2$ occurred. During an increase of temperature to 280 °C, $ZnCl_2$ catalytically assists the cellulose degradation through hydrolysis, oxidative degradation, and further dehydration, along with swelling of the biomass structure that led to mesoporous structures. From temperature 280–400 °C further pore formation and aromatization of carbon structure occurs, and further increase of temperature lead to decomposition and vaporization of $ZnCl_2$ and pore development via formation spaces between carbon layers. At a high $ZnCl_2$ ratio as activating agent, it is also known that pore widening is the dominant mechanism during the activation, resulting in wide distribution of pore size, as obtained in AC-0. Similar results have been reported by previous researchers [39, 40]. On the other hand, HTC with $ZnCl_2$ catalyst affects the pore development in the AC. As previously mentioned, the AC-1 to AC-3 possessed pores ranging from 2–10 nm with narrower distribution than AC-0.

The pore characteristics of AC samples are presented in Table 2. It could be seen that all AC samples in this study possessed higher surface area compared to commercial AC (Merck). Furthermore, it could be seen that the use of a catalyst during HTC process gave an effect on the surface area of AC samples, with the highest surface area of 1954 and 1885 m^2/g obtained for AC-200-3 and AC-225-2 samples respectively, compared with AC-200-0 (1165 m^2/g) and AC-225-0 (1694 m^2/g). Compared to AC-225 samples, the difference in surface area for AC-200-0 and AC-200-3 is more notable with an increase of surface area almost two times (~790 m^2/g) compared to the one without any catalyst. As previously mentioned, during HTC, $ZnCl_2$ could act as a Lewis acid that catalyzes the scission of glycosidic bonds in cellulose structure starting from a temperature of 200 °C [27]. Without a catalyst, the HTC temperature was the only factor that influence the hydrolysis of CPH and resulted in different pore structures. Higher carbonization temperature is known to be more beneficial in the pore formation of the HC [11], while the initial pore formation in HC is essential to promote a more porous structure of the AC [41]. This could explain the observation of a higher surface area of AC-225-0 compared to AC-200-0. Furthermore, for both temperatures, various catalyst ratios gave a relatively close surface area of around 1750–1950 m^2/g. Thus, it could be seen that the effect of catalyst addition is more profound at a lower HTC temperature of 200 °C.

These results obtained were in line with previous studies. MacDermid-Watts et al. [17] reported an increase of 200 m^2/g surface area of AC sample without catalyst and with $FeCl_3$ catalyst in the synthesis of AC from corn distiller's fibers. A similar result was also reported by Wu et al. [42] during synthesizing AC from lignin, where an increase of surface area up to 300 m^2/g was observed with the addition of $ZnCl_2$ during HTC. Susanti et al. [16] also reported an increase of AC surface area of ~300 m^2/g for sample obtained from $CeCl_3$ catalyzed HTC combined with KOH chemical activation, compared to one without catalyst.

3.5 Crystallinity of AC

The XRD diffractograms of AC samples are presented in Fig. 6. It shows that there are two broad peaks observed in all AC samples, indicating the amorphous nature of the AC samples. The broad peaks centered around 26.5° and 43° correspond to the (002) and (100) planes of graphitic carbon structure, respectively. Furthermore, there are some ZnO peaks observed in the AC-0 samples that might come from an imperfect washing process. The $ZnCl_2$ was impregnated into the biomass and hydrolyzed to $H[ZnCl_2(OH)]$ during the impregnation step. During activation at 600 °C, the $H[ZnCl_2(OH)]$ was decomposed into ZnO and HCl.

A comparison of this work with previous studies under similar synthesis methods (HTC and pyrolysis) is presented in Table 3 [20, 41–43]. It could be observed that the AC synthesized from CPH with the combination of

Table 2 Pore characteristics of AC samples

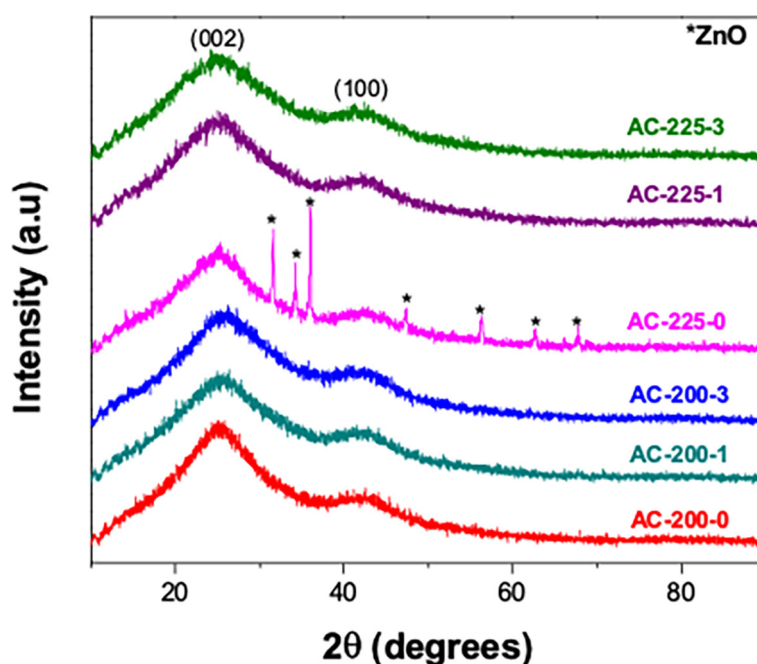| Sample	BET surface area (m^2/g)	Average pore diameter (nm)	Total pore volume (cm^3/g)	Mesopore volume* (cm^3/g)
Commercial AC	719	3.3	0.4871	0.3726
AC-200-0	1165	2.0	1.4711	1.2649
AC-200-1	1859	3.1	1.4249	1.0362
AC-200-2	1899	3.1	1.4659	1.0743
AC-200-3	1954	2.3	1.1173	0.7423
AC-225-0	1695	2.9	1.2203	0.8173
AC-225-1	1749	3.2	1.3775	1.0181
AC-225-2	1885	3.0	1.4316	1.0253
AC-225-3	1870	3.0	1.4241	1.0277

*Based on BJH analysis measured from 2 to 50 nm

Fig. 6 XRD diffractograms of AC samples

Table 3 Comparison of the surface area of various AC reported in the literature

| Precursor | HTC | | | Pyrolysis | | | Surface area (m^2/g) | Ref. |
	Catalyst	Ratio (biomass: catalyst)	Condition	Activating agent	Ratio (char: activating agent)	Condition		
CPH	$ZnCl_2$	1:3	200 °C, 24 h	$ZnCl_2$	1:4	600 °C, 1 h	1955	This study
Wheat straw	$ZnCl_2$	1:2	200 °C, 24 h	H_3PO_4	1:2	500 °C, 1 h	1258	[20]
Coconut shell	$ZnCl_2$	1:2	275 °C, 53 bar, 20 min	CO_2	-	800 °C, 2 h	1652	[41]
Lignin	$ZnCl_2$	1:2	180 °C, 10 h	KOH	1:3	700 °C, 1.5 h	2592	[42]
Sugarcane bagasse	$FeCl_3$	1:4	200 °C, 3 h	-	-	800 °C, 1 h	403	[43]

$ZnCl_2$-catalyzed HTC and $ZnCl_2$ chemical activation treatment could give a comparable surface area with other AC from various precursors. In addition, it showed that CPH synthesized by the combination of HTC and chemical activation shows much better surface area compared with the combination of pyrolysis carbonization and chemical activation only (780 and 642 m^2/g) [44, 45]. The high surface area AC obtained in this study make the AC from CPH with the combination of $ZnCl_2$ catalyzed HTC and $ZnCl_2$ chemical activation a prospective material for various application such as adsorbent [46], catalyst support [47], and supercapacitor electrode [48].

4 Conclusion

In this study, the effect of HTC temperature and $ZnCl_2$ as a catalyst during HTC process on the characteristic of AC

was investigated. $ZnCl_2$ could act as a Lewis acid catalyst that assists the hydrolysis process during HTC, as indicated in the FTIR analysis and the decrease of HC yield with the increase of catalyst concentration. Further conversion of HC to AC was done by using chemical activation at the same HC:$ZnCl_2$ ratio of 1:4 and heating at 600 °C for 1 h. It could be observed that different morphology of AC was obtained for AC samples with and without catalyst, whereas with $ZnCl_2$ catalyst, the AC had a porous structure decorated with carbon microsphere. Furthermore, the effect of the catalyst on the AC surface area is more profound at HTC temperature of 200 °C as shown in the high difference in the AC-200-3 surface area of 1954 m^2/g compared to one without catalyst (1165 m^2/g). The increase in the surface area could come from the initial porous structure of catalyzed HC could help in the development

of AC pores during chemical activation. Furthermore, more oxygenated functional groups were detected in both AC-200-3 and AC-225-3 samples compared to AC-200-0 and AC-225-0, with similar diffraction patterns for all AC samples. This research also highlights that the carbonization temperature, and the addition of a catalyst are two variables that need to be optimized. The results obtained in this study could become a promising method to synthesize AC with superior characteristics.

References

[1] International Cocoa Organization "August 2021 Quarterly Bulletin of Cocoa Statistics", 2021. [online] Available at: https://www.icco.org/august-2021-quarterly-bulletin-of-cocoa-statistics/ [Accessed: 12 September 2021]

[2] Biehl, B., Ziegleder, G. "COCOA: Production, Products, and Use", In: Caballero, B. (ed.) Encyclopedia of Food Sciences and Nutrition, Academic Press, 2003, pp. 1448–1463. ISBN 978-0-12-227055-0
https://doi.org/10.1016/B0-12-227055-X/00262-5

[3] Campos-Vega, R., Nieto-Figueroa, K. H., Oomah, B. D. "Cocoa (*Theobroma cacao* L.) pod husk: Renewable source of bioactivecompounds", Trends Food Science & Technology, 81, pp. 172–184, 2018.
https://doi.org/10.1016/j.tifs.2018.09.022

[4] Vriesmann, L. C., Teófilo, R. F., Lúcia de Oliveira Petkowicz, C. "Extraction and characterization of pectin from cacao pod husks (*Theobroma cacao* L.) with citric acid", LWT - Food Science and Technology, 49(1), pp. 108–116, 2012.
https://doi.org/10.1016/j.lwt.2012.04.018

[5] Susanti, R. F., Alvin, S., Kim, J. "Toward high-performance hard carbon as an anode for sodium-ion batteries: Demineralization of biomass as a critical step", Journal of Industrial and Engineering Chemistry, 91, pp. 317–329, 2020.
https://doi.org/10.1016/j.jiec.2020.08.016

[6] Susanti, R. F., Kevin, G., Erico, M., Kevien, Andreas, A., Kristianto, H., Handoko, T. "Delignification, Carbonization Temperature and Carbonization Time Effects on the Hydrothermal Conversion of Salacca Peel", Journal of Nanoscience and Nanotechnology, 18(10), pp. 7263–7268, 2018.
https://doi.org/10.1166/jnn.2018.15724

[7] Susanti, R. F., Wiratmadja, R. G. R., Kristianto, H., Arie, A. A., Nugroho, A. "Synthesis of high surface area activated carbon derived from cocoa pods husk by hydrothermal carbonization and chemical activation using zinc chloride as activating agent", Materials Today: Proceedings, 63(Supplement 1), pp. S55–S60, 2022.
https://doi.org/10.1016/j.matpr.2022.01.042

[8] Correa, C. R., Hehr, T., Voglhuber-Slavinsky, A., Rauscher, Y., Kruse, A. "Pyrolysis vs. hydrothermal carbonization: Understanding the effect of biomass structural components and inorganic compounds on the char properties", Journal of Analytical and Applied Pyrolysis, 140, pp. 137–147, 2019.
https://doi.org/10.1016/j.jaap.2019.03.007

[9] Funke, A., Ziegler, F. "Hydrothermal carbonization of biomass: A summary and discussion of chemical mechanisms for process engineering", Biofuels, Bioproducts and Biorefining, 4(2), pp. 160–177, 2010.
https://doi.org/10.1002/bbb.198

[10] MacDermid-Watts, K., Pradhan, R., Dutta, A. "Catalytic Hydrothermal Carbonization Treatment of Biomass for Enhanced Activated Carbon: A Review", Waste and Biomass Valorization, 12(5), pp. 2171–2186, 2021.
https://doi.org/10.1007/s12649-020-01134-x

[11] Susanti, R. F., Arie, A. A., Kristianto, H., Erico, M., Kevin, G., Devianto, H. "Activated carbon from citric acid catalyzed hydrothermal carbonization and chemical activation of salacca peel as potential electrode for lithium ion capacitor's cathode", Ionics, 25(8), pp. 3915–3925, 2019.
https://doi.org/10.1007/s11581-019-02904-x

[12] Ameen, M., Zamri, N. M., May, S. T., Azizan, M. T., Aqsha, A., Sabzoi, N., Sher, F. "Effect of acid catalysts on hydrothermal carbonization of Malaysian oil palm residues (leaves, fronds, and shells) for hydrochar production", Biomass Conversion and Biorefinery, 12(1), pp. 103–114, 2021.
https://doi.org/10.1007/s13399-020-01201-2

[13] Zhang, S., Sheng, K., Yan, W., Liu, J., Shuang, E., Yang, M., Zhang, X. "Bamboo derived hydrochar microspheres fabricated by acid-assisted hydrothermal carbonization", Chemosphere, 263, 128093, 2021.
https://doi.org/10.1016/j.chemosphere.2020.128093

[14] Li, Y., Huang, Z.-H., Kang, F.-Y., Li, B.-H. "Preparation of activated carbon microspheres from phenolic resin with metal compounds by sub- and supercritical water activation", New Carbon Materials, 25(2), pp. 109–113, 2010.
https://doi.org/10.1016/S1872-5805(09)60019-6

[15] Ondy, F. C., Chrismanto, C., Susanti, R. F., Kristianto, H., Devianto, H. "Preparation of Salacca Peel Based Activated Carbon using CeCl₃ Catalyzed ydrothermal Carbonization and Microwave Induced KOH Chemical Activation as Ni-Ion Capacitor Electrode", IOP Conference Series: Materials Science and Engineering, 742(1), 012045, 2020.
https://doi.org/10.1088/1757-899X/742/1/012045

[16] Susanti, R. F., Kristianto, H., Chrismanto, C., Ondy, F. C., Kim, J., Chang, W. "Cerium chloride-assisted subcritical water carbonization for fabrication of high-performance cathodes for lithium-ion capacitors", Journal of Applied Electrochemistry, 51(10), pp. 1449–1462, 2021.
https://doi.org/10.1007/s10800-021-01591-9

[17] MacDermid-Watts, K., Adewakun, E., Norouzi, O., Abhi, T. D., Pradhan, R., Dutta, A. "Effects of FeCl$_3$ Catalytic Hydrothermal Carbonization on Chemical Activation of Corn Wet Distillers' Fiber", ACS Omega, 6(23), pp. 14875–14886, 2021.
https://doi.org/10.1021/acsomega.1c00557

[18] Hasan, R. O., Ercan, B., Acikkapi, A. N., Ucar, S., Karagöz, S. "Effects of Metal Chlorides on the Hydrothermal Carbonization of Grape Seeds", Energy & Fuels, 35(10), pp. 8834–8843, 2021.
https://doi.org/10.1021/acs.energyfuels.1c00954

[19] Li, F., Zimmerman, A. R., Hu, X., Yu, Z., Huang, J., Gao, B. "One-pot synthesis and characterization of engineered hydrochar by hydrothermal carbonization of biomass with ZnCl$_2$", Chemosphere, 254, 126866, 2020.
https://doi.org/10.1016/j.chemosphere.2020.126866

[20] Xing, X., Jiang, W., Li, S., Zhang, X., Wang, W. "Preparation and analysis of straw activated carbon synergetic catalyzed by ZnCl$_2$-H$_3$PO$_4$ through hydrothermal carbonization combined with ultrasonic assisted immersion pyrolysis", Waste Management, 89, pp. 64–72, 2019.
https://doi.org/10.1016/j.wasman.2019.04.002

[21] Kristianto, H., Lavenki, Y., Susanti, R. F. "Synthesis and Characterization of Activated Carbon Derived from Salacca Peel Using ZnCl$_2$ Hydrothermal Carbonization and Chemical Activation with Microwave Heating", IOP Conference Series: Materials Science and Engineering, 742(1), 012044, 2020.
https://doi.org/10.1088/1757-899X/742/1/012044

[22] Guo, S., Gao, Y., Wang, Y., Liu, Z., Wei, X., Peng, P., Xiao, B., Yang, Y. "Urea/ZnCl$_2$ in situ hydrothermal carbonization of *Camellia sinensis* waste to prepare N-doped biochar for heavy metal removal", Environmental Science and Pollution Research, 26(29), pp. 30365–30373, 2019.
https://doi.org/10.1007/s11356-019-06194-8

[23] Mohammed, I. S., Na, R., Kushima, K., Shimizu, N. "Investigating the Effect of Processing Parameters on the Products of Hydrothermal Carbonization of Corn Stover", Sustainability, 12(12), 5100, 2020.
https://doi.org/10.3390/su12125100

[24] Chowdhury, Z. Z., Krishnan, B., Sagadevan, S., Rafique, R. F., Hamizi, N. A. B., Abdul Wahab, Y., Khan, A. A., Johan, R. B., Al-douri, Y., Kazi, S. N., Tawab Shah, S. "Effect of Temperature on the Physical, Electro-Chemical and Adsorption Properties of Carbon Micro-Spheres Using Hydrothermal Carbonization Process", Nanomaterials, 8(8), 597, 2018.
https://doi.org/10.3390/nano8080597

[25] Chen, C., Liang, W., Fan, F., Wang, C. "The Effect of Temperature on the Properties of Hydrochars Obtained by Hydrothermal Carbonization of Waste Camellia oleifera Shells", ACS Omega, 6(25), pp. 16546–16552, 2021.
https://doi.org/10.1021/acsomega.1c01787

[26] Lua, A. C., Yang, T. "Characteristics of activated carbon prepared from pistachio-nut shell by zinc chloride activation under nitrogen and vacuum conditions", Journal of Colloid and Interface Science, 290(2), pp. 505–513, 2005.
https://doi.org/10.1016/j.jcis.2005.04.063

[27] Amarasekara, A. S., Ebede, C. C. "Zinc chloride mediated degradation of cellulose at 200 °C and identification of the products", Bioresource Technology, 100(21), pp. 5301–5304, 2009.
https://doi.org/10.1016/j.biortech.2008.12.066

[28] Shen, W., Li, Z., Liu, Y. "Surface Chemical Functional Groups Modification of Porous Carbon", Recent Patents on Chemical Engineering, 1(1), pp. 27–40, 2008.
https://doi.org/10.2174/2211334710801010027

[29] Chun, K. S., Husseinsyah, S., Osman, H. "Modified cocoa pod husk-filled polypropylene composites by using methacrylic acid", BioResources, 8(3), pp. 3260–3275, 2013.
https://doi.org/10.15376/biores.8.3.3260-3275

[30] Hong, D., Zhou, J., Hu, C., Zhou, Q., Mao, J., Qin, Q. "Mercury removal mechanism of AC prepared by one-step activation with ZnCl$_2$", Fuel, 235, pp. 326–335, 2019.
https://doi.org/10.1016/j.fuel.2018.07.103

[31] Chen, J., Zhang, L., Yang, G., Wang, Q., Li, R., Lucia, L. A. "Preparation and Characterization of Activated Carbon from Hydrochar by Phosphoric Acid Activation and its Adsorption Performance in Prehydrolysis Liquor", Bioresources, 12(3), pp. 5928–5941, 2017.
https://doi.org/10.15376/biores.12.3.5928-5941

[32] Tiegam, R. F. T., Tchuifon Tchuifon, D. R., Santagata, R., Kouteu Nanssou, P. A., Anagho, S. G., Ionel, I., Ulgiati, S. "Production of activated carbon from cocoa pods: Investigating benefits and environmental impacts through analytical chemistry techniques and life cycle assessment", Journal of Cleaner Production, 288, 125464, 2021.
https://doi.org/10.1016/j.jclepro.2020.125464

[33] Arie, A. A., Kristianto, H., Halim, M., Lee, J. K. "Synthesis and modification of activated carbon originated from Indonesian local Orange peel for lithium ion Capacitor's cathode", Journal of Solid State Electrochemistry, 21(5), pp. 1331–1342, 2017.
https://doi.org/10.1007/s10008-016-3445-7

[34] Wang, T., Zhai, Y., Zhu, Y., Li, C., Zeng, G. "A review of the hydrothermal carbonization of biomass waste for hydrochar formation: Process conditions, fundamentals, and physicochemical properties", Renewable and Sustainable Energy Reviews, 90, pp. 223–247, 2018.
https://doi.org/10.1016/j.rser.2018.03.071

[35] Cychosz, K. A., Guillet-Nicolas, R., García-Martınez, J., Thommes, M. "Recent advances in the textural characterization of hierarchically structured nanoporous materials", Chemical Society Reviews, 46(2), pp. 389–414, 2017.
https://doi.org/10.1039/C6CS00391E

[36] Ma, G., Guo, D., Sun, K., Peng, H., Yang, Q., Zhou, X., Zhao, X., Lei, Z. "Cotton-based porous activated carbon with a large specific surface area as an electrode material for high-performance supercapacitors", RSC Advances, 5(79), pp. 64704–64710, 2015.
https://doi.org/10.1039/C5RA11179J

[37] Thommes, M., Kaneko, K., Neimark, A. V., Olivier, J. P., Rodriguez-Reinoso, F., Rouquerol, J., Sing, K. S. W. "Physisorption of gases, with special reference to the evaluation of surface area and pore size distribution (IUPAC Technical Report)", Pure Applied Chemistry, 87(9–10), pp. 1051–1069, 2015.
https://doi.org/10.1515/pac-2014-1117

[38] Xia, M., Shao, X., Sun, Z., Xu, Z. "Conversion of cotton textile wastes into porous carbons by chemical activation with $ZnCl_2$, H_3PO_4, and $FeCl_3$", Environmental Science and Pollution Research, 27(20), pp. 25186–25196, 2020.
https://doi.org/10.1007/s11356-020-08873-3

[39] Okhovat, A., Ahmadpour, A. "A Comparative Study of the Effects of Different Chemical Agents on the Pore-Size Distributions of Macadamia Nutshell-Based Activated Carbons Using Different Models", Adsorption Science & Technology, 30(2), pp. 159–169, 2012.
https://doi.org/10.1260/0263-6174.30.2.159

[40] Du, X., Zhao, W., Ma, S., Ma, M., Qi, T., Wang, Y., Hua, C. "Effect of $ZnCl_2$ impregnation concentration on the microstructure and electrical performance of ramie-based activated carbon hollow fiber", Ionics, 22(4), pp. 545–553, 2016.
https://doi.org/10.1007/s11581-015-1571-3

[41] Jain, A., Jayaraman, S., Balasubramanian, R., Srinivasan, M. P. "Hydrothermal pre-treatment for mesoporous carbon synthesis: enhancement of chemical activation", Journal of Materials Chemistry A, 2(2), pp. 520–528, 2014.
https://doi.org/10.1039/C3TA12648J

[42] Wu, Y., Cao, J.-P., Zhao, X.-Y., Zhuang, Q.-Q., Zhou, Z., Huang, Y., Wei, X.-Y. "High-performance electrode material for electric double-layer capacitor based on hydrothermal pre-treatment of lignin by $ZnCl_2$", Applied Surface Science, 508, 144536, 2020.
https://doi.org/10.1016/j.apsusc.2019.144536

[43] Diaz de Tuesta, J. L., Saviotti, M. C., Roman, F. F., Pantuzza, G. F., Sartori, H. J. F., Shinibekova, A., Kalmakhanova, M. S., Massalimova, B. K., Pietrobelli, J. M. T. A., Lenzi, G. G., Gomes, H. T. "Assisted hydrothermal carbonization of agroindustrial byproducts as effective step in the production of activated carbon catalysts for wet peroxide oxidation of micro-pollutants", Journal of Environmental Chemical Engineering, 9(1), 105004, 2021.
https://doi.org/10.1016/j.jece.2020.105004

[44] Cruz, G., Pirilä, M., Huuhtanen, M., Carrión, L., Alvarenga, E., Keiski, R. "Production of Activated Carbon from Cocoa (*Theobroma cacao*) Pod Husk", Journal of Civil & Environmental Engineering, 2(2), 109, 2012.
https://doi.org/10.4172/2165-784X.1000109

[45] Pereira, R. G., Veloso, C. M., da Silva, N. M., de Sousa, L. F., Bonomo, R. C. F., de Souza, A. O., Souza, M. O. d. G., Fontan, R. d. C. I. "Preparation of activated carbons from cocoa shells and siriguela seeds using H_3PO_4 and $ZnCL_2$ as activating agents for BSA and α-lactalbumin adsorption", Fuel Processing Technology, 126, pp. 476–486, 2014.
https://doi.org/10.1016/j.fuproc.2014.06.001

[46] Hameed, B. H., Ahmad, A. L., Latiff, K. N. A. "Adsorption of basic dye (methylene blue) onto activated carbon prepared from rattan sawdust", Dyes and Pigments, 75(1), pp. 143–149, 2007.
https://doi.org/10.1016/j.dyepig.2006.05.039

[47] Iwanow, M., Gärtner, T., Sieber, V., König, B. "Activated carbon as catalyst support: precursors, preparation, modification and characterization", Belstein Journal of Organic Chemistry, 16, pp. 1188–1202, 2020.
https://doi.org/10.3762/bjoc.16.104

[48] Maher, M., Hassan, S., Shoueir, K., Yousif, B., Abo-Elsoud, M. E. A. "Activated carbon electrode with promising specific capacitance based on potassium bromide redox additive electrolyte for supercapacitor application", Journal of Materials Research and Technology, 11, pp. 1232–1244, 2021.
https://doi.org/10.1016/j.jmrt.2021.01.080